JOURNAL OF SOLID STATE CHEMISTRY 115, 313–323 (1995)

Synthesis, Crystal Structure, and Ionic Conductivity of a Polycrystalline Lithium Phosphorus Oxynitride with the γ-Li_3PO_4 Structure

B. Wang, B. C. Chakoumakos, B. C. Sales, B. S. Kwak, and J. B. Bates

Solid State Division, Oak Ridge National Laboratory, Oak Ridge, Tennessee 37831-6030

Received April 18, 1994; in revised form August 1, 1994; accepted August 3, 1994

A crystalline form of lithium phosphorus oxynitride, $Li_{2.88}PO_{3.73}N_{0.14}$, has been prepared by solid state reaction between Li_3N and $LiPO_3$ under a flowing N_2 atmosphere. The structure of the oxynitride was refined by Rietveld analysis of neutron powder diffraction data using the orthorhombic unit cell of γ-Li_3PO_4 with space group *Pmnb*. High-performance liquid chromatography measurement indicates that most nitrogen substitutes for oxygen to form PO_3N structural units with small concentrations of P—N=P due to some Li ↔ P disorder in the structure. The ionic conductivity of $Li_{2.88}PO_{3.73}N_{0.14}$ ($\sigma_{25°C} \sim 10^{-13}$ S · cm^{-1}) is several orders of magnitude higher than that of γ-Li_3PO_4 ($\sigma_{25°C} \sim 10^{-18}$ S · cm^{-1}).

INTRODUCTION

It has been shown in recent work in this laboratory that the addition of nitrogen into the structure of amorphous lithium phosphate thin films deposited by sputtering Li_3PO_4 in N_2 increases the lithium ion conductivity by a factor of about 40 (1, 2). More importantly, the lithium phosphorus oxynitride electrolyte is stable in contact with metallic lithium at high potentials enabling the development of rechargeable thin film lithium batteries (3). During the investigation of bulk glasses in the Li_2O–PON–P_2O_5 system, we succeeded in synthesizing a crystalline form of lithium phosphorus oxynitride. In this paper, we report the synthesis, crystal structure refinement, and ionic conductivity of this material which has the composition $Li_{2.88}PO_{3.73}N_{0.14}$ and the structure of γ-Li_3PO_4. Juszczyk and Podsialdo (4) claimed to have synthesized a crystalline compound with the composition Li_3PON_2 but provided no diffraction data to support this claim. Otherwise, we have not found any other published report of the preparation of a crystalline lithium phosphorus oxynitride.

EXPERIMENTAL PROCEDURES

The objective of the synthesis was to obtain a crystalline lithium phosphorus oxynitride with the same 3 : 1 Li : P ratio as Li_3PO_4. The first attempts were made by reacting Li_2O and P_3N_5, but only multiphase products were formed. A material of a single crystalline phase was obtained by a solid state reaction between Li_3N (Alfa, 99.5%) and $LiPO_3$ (Alfa, 98%)[1] at a molar ratio of 2/3 : 1. After mixing exact molar ratios of the reactants in an agate mortar in an argon-filled glove box, the mixture was packed in an alumina crucible and transferred to a nitrogen-filled glove bag in a sealed box. Inside the glove bag, the alumina crucible containing the mixture was loaded into a stainless steel furnace liner which was then closed by compressing a top flange against an O-ring seal (Fig. 1). The solid state reaction was carried out by heating the mixture at 600°C for 24 hr under a flowing N_2 atmosphere.[2] Samples of γ-Li_3PO_4 were prepared by heating Li_3PO_4 (Alfa, 99%) at 800°C for 24 hr and cooling slowly to room temperature at the rate of −1°C/min.

The nitrogen content in the sample was estimated from the total weight gain during a thermal gravimetric analysis (TGA) measurement performed in a Perkin–Elmer TGS-2 system. About 8 mg of the sample powder was heated at 5°C/min to 700°C in a flowing oxygen atmosphere and held for ~150 hr before cooling to room temperature. Powder X-ray diffraction (PXRD) measurements of the oxynitride and γ-Li_3PO_4 samples were made with a Scintag diffractometer equipped with a high-purity Ge detector using Cu$K\alpha$ radiation. Data were collected in the 2θ range of 10°–70° with a 2θ step size of 0.03° and a counting time of 4 sec/step. It was found that the diffraction pattern for the synthesized lithium phosphorus oxynitride was similar to that of γ-Li_3PO_4 (5).

Neutron diffraction data for the oxynitride and γ-Li_3PO_4 were collected using the HB4 powder diffractometer at the high-flux isotope reactor at ORNL. A full description of the instrument design and the experimental details are

[1] The major impurity is LiH_2PO_4, 1.95%.

[2] Based on the O_2, CO_2, H_2O, and H_2 impurity content (20, 5, 5 and 5 ppm), $P_{O_2} \approx 2 \times 10^{-5}$ atm at 600°C.

0022-4596/95 $6.00

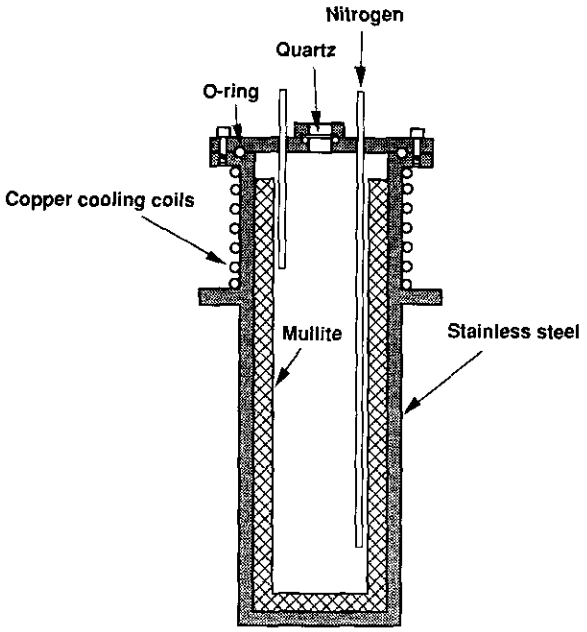

FIG. 1. Stainless steel furnace liner with O-ring seals used in the preparation of lithium phosphorus oxynitride.

given elsewhere (6). The neutron wavelength was determined to be 1.416 Å from refinements of a nickel powder standard. Data were collected from samples contained in vanadium cans at 295 K over the 2θ range of 11° to 135° in steps of 0.05°. The structural refinements were made using the computer program GSAS (7), which employs the Rietveld method (8). The pseudo-Voigt peak-profile function truncated at 0.5% of the peak height as described by Thompson *et al.* (9) was used, incorporating five terms. Peak asymmetry and sample displacement parameters were also refined. The background was defined by a cosine Fourier series with four terms. Further details of the refinement methodology are given in Ref. (7). The coherent scattering lengths used were: Li (−2.14 fm), P (5.81 fm), O (5.13 fm), and N (9.30 fm) from Ref. (10). Intensities were corrected for the Lorentz effect. The data sets were limited to the 2θ angular range of 14° to 132° or to d-spacing of 5.809 to 0.7750 Å. The function minimized in the least-squares procedure was $\Sigma w_i(Y_{io} - Y_{ic})^2$, where Y_{io} and Y_{ic} are the observed and calculated intensities at each step i in the pattern. The weight w_i assigned to each step intensity is the reciprocal of the variance σ_i^2 at the ith step and was evaluated by $w_i = 1/\sigma_i^2 \approx n/Y_{io}$ where n is the number of detectors contributing to the average step intensity. The following agreement factors were calculated,

$$R_p = \Sigma|Y_{io} - Y_{ic}|\Sigma Y_{io},$$

$$R_{wp} = [\Sigma w_i(Y_{io} - Y_{ic})^2/\Sigma w_i Y_{io}^2]^{1/2},$$

$$\text{Goodness-of-fit} = \Sigma w_i(Y_{io} - Y_{ic})^2/(N - P),$$

where N and P are the number of observations and adjustable parameters, respectively.

Starting values for the structural parameters for the refinement of the $Li_{2.88}PO_{3.73}N_{0.14}$ structure were obtained from the structure data of the medium-temperature γ-form of Li_3PO_4 (11). In all, 35 parameters were refined, and the least-squares refinements were continued until the sum of the squared errors, i.e., (parameter shifts/estimated standard deviations)^2, was less than 1%.

High-performance liquid chromatography (HPLC) was used to determine the distribution of phosphate anions in $Li_{2.88}PO_{3.73}N_{0.14}$ (12). Approximately 1-mg samples of the oxynitride and γ-Li_3PO_4 were dissolved in 10 ml of an aqueous solution of 0.22 M NaCl and 5 mM Na_4EDTA, and a small quantity of this solution was injected upstream from an Animex A-27 ion exchange column. The column was subsequently flushed with a NaCl solvent using a delivery system which was programmed to increase linearly the NaCl concentration in the solvent stream from 0.28 to 0.53 M over a 40-min interval. The polyphosphate anions bound on the column were released in the order of increasing molecular weight, such as the sequence P_1, P_2, where $P_1 = PO_4^{3-}$ and $P_2 = P_2O_7^{4-}$. As the anions were released from the column, they were converted to phosphate monomers and complexed with molybdenum [Mo(V)–Mo(VI)]. The complex was detected by measuring the optical absorption of the solvent stream at 660 nm.

X-ray photoelectron spectroscopy (XPS) was used to measure the core levels of Li, P, N, and O in the oxynitride and the starting materials $LiPO_3$ and Li_3N. The photoelectron spectra were obtained with a PHI 5000 ESCA system using 1487 eV Al$K\alpha$ X-rays as the excitation source. Prior to loading into the analysis chamber, the samples were ground in a nitrogen atmosphere to obtain spectra reasonably characteristic of bulk composition ($LiPO_3$ and $Li_{2.88}PO_{3.73}N_{0.14}$) or loaded as received in the glove box filled with high purity argon (Li_3N). It was observed that grinding the $LiPO_3$ sample in a nitrogen atmosphere actually reduced surface nitrogen contamination. After grinding, the average grain size of the samples was reduced from ~50 to ~2 μm as determined by scanning electron microscopy (SEM). Survey scans were made from 1000 to 0 eV, and high resolution spectra were taken in the O_{1s}, N_{1s}, P_{2p}, Li_{1s}, and C_{1s} regions. These core level spectra were referenced to the C_{1s} line at 285.0 eV. Curve fitting of the N_{1s} peak was performed by varying the intensity of each component and the binding energy while keeping the full-width-half-maximum (FWHM) constant.

Impedance measurements were made at frequencies from 0.1 Hz to 50 KHz using a Solartron 1250 frequency response analyzer, with signals of 50 mV p-p applied to

the samples (1, 2). Samples for these measurements were made by cold pressing finely ground powders into a pellet and sintering the pellet at 500°C in flowing N_2 (oxynitride) or in air (γ-Li_3PO_4). After sintering, the pellets measured about 0.2 cm thick by 1.0 cm in diameter with densities of 1.79 (oxynitride) and 1.69 g/cm^3 (γ-Li_3PO_4). Platinum contacts about 2000 Å thick were deposited onto the faces of the pellets by sputtering. A pellet was sandwiched between Pt plates and pressed against a heater block inside a small vacuum chamber, and a thermocouple was attached to the heater block near the pellet. High purity argon was circulated through the chamber during the impedance measurements which were made at 10 and 20°C increments from 100 to 300°C with increasing and decreasing temperatures.

RESULTS AND DISCUSSION

The ratio of lithium to phosphorus in the oxynitride determined from the refinement of the neutron diffraction data is Li : P = 2.88 (±0.04). With the measured mass gain of 1.5 (±0.08)% obtained from the TGA analysis, the composition of the sample is $Li_{2.88}PO_{3.73}N_{0.14}$ assuming that all of the nitrogen is in the crystalline phase (see below) and that the oxygen required for charage balance is present. Apparently due to the loss of nitrogen from the high temperature required for the solid state reaction, the nitrogen content is significantly lower than expected for oxidation of the theoretical end product $Li_3PO_3N_{2/3}$ ($2/3Li_3N + LiPO_3 \rightarrow Li_3PO_3N_{2/3}$) to Li_3PO_4. The composition of the crystalline lithium phosphorus oxynitride is displayed in the $LiO_{0.5}$–PON–$PO_{2.5}$ phase diagram in Fig. 2 along with our previously studied amorphous lithium phosphorus oxynitride thin films (1), bulk lithium phosphorus oxynitride glasses prepared in our laboratory (13), and bulk lithium phosphorus oxynitride glasses studied by Boukbir and Marchand (14). It can be seen that the composition of the crystalline oxynitride is closer to that of the amorphous thin films than to the bulk glasses.

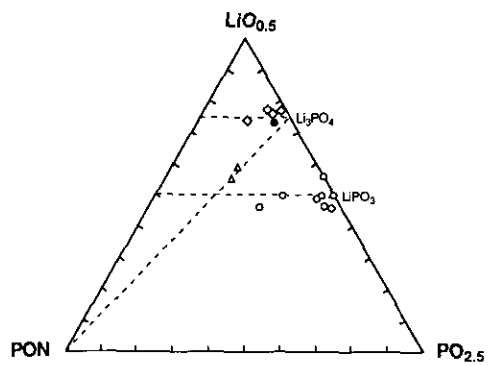

FIG. 2. Phase diagram of $LiO_{0.5}$–PON–$PO_{2.5}$ showing the compositions of crystalline lithium phosphorus oxynitride (●), amorphous lithium phosphorus oxynitride thin films (◇) (1), bulk lithium phosphorus oxynitride glasses prepared in our laboratory (○) (13), and bulk lithium phosphorus oxynitride glasses studied by Boukbir and Marchand (△) (14).

Three polymorphs of Li_3PO_4 are known to occur with progressively higher temperature: β, γ, and α-Li_3PO_4. On heating, β-Li_3PO_4 transforms to the γ-Li_3PO_4 at 520°C, and γ-Li_3PO_4 transforms to α-Li_3PO_4 at 1170°C which is stable up to the melting point (15). β-Li_3PO_4 has a wurtzite superstructure in which both Li and P are in tetrahedral sites and all the tetrahedra share corners and point in the same direction (Fig. 3). For γ-Li_3PO_4, on the other hand, some tetrahedra point in the opposite direction (Fig. 4), similar to SiO_4 tetrahedra in an olivine structure (16). Each oxygen in β- and γ-Li_3PO_4 is shared by three LiO_4 tetrahedra and one PO_4 tetrahedron (Figs. 3 and 4). A major difference between these two structures is that some edge-sharing of LiO_4 tetrahedra occurs in γ-Li_3PO_4 (Fig. 5), whereas in β-Li_3PO_4 there are only corner-linked tetrahedra (Fig. 3). A complete structural description of α-Li_3PO_4 has not been given because this polymorph cannot be quenched to room temperature. On the basis of high temperature diffractometry, Reculeau *et al.* (15) suggested that α-Li_3PO_4 also has a wurtzite superstructure, but one that is distinctly different from that of β-Li_3PO_4.

The structure of γ-Li_3PO_4 has space group symmetry *Pmnb*, with $Z = 4$. Six atoms occupy the asymmetric unit: three tetrahedral cations Li(1), Li(2), and P; and three oxygen anions. There are twice as many Li(1) tetrahedra as Li(2) tetrahedra. Running along the **a** direction, each Li(2) tetrahedra shares adjacent edges with two Li(1) tetrahedra which in turn only share corners with other Li(1) tetrahedra (Fig. 5a). Initially it was thought that the nitrogen content of the oxynitride was high so that, given the large difference in the scattering lengths of nitrogen and oxygen, the Rietveld refinement could reveal directly how much nitrogen was substituted into the sample and at which oxygen sites. However, because the actual nitrogen content was much lower and the crystallinity of the sample prepared was sufficiently poor, attempts to refine the (N, O) content of the oxygen sites did not lead to significant improvements. Unconstrained refinements of the oxygen site occupancies always lead to values somewhat larger than 1, which suggests that an element with a larger scattering length such as N is substituted at all three oxygen sites. The occupancies of all three tetrahedral sites resulting from unconstrained refinements are each significantly less than 1. The *R*-factors are significantly lower for this model, but the goodness-of-fit is unchanged. Moreover, the temperature factors for the Li(1) and P sites become grossly negative. The occupations and temperature factors are strongly correlated as is well known. Even with the temperature factors fixed at reasonable values the tetrahedral sites are not refined to be fully

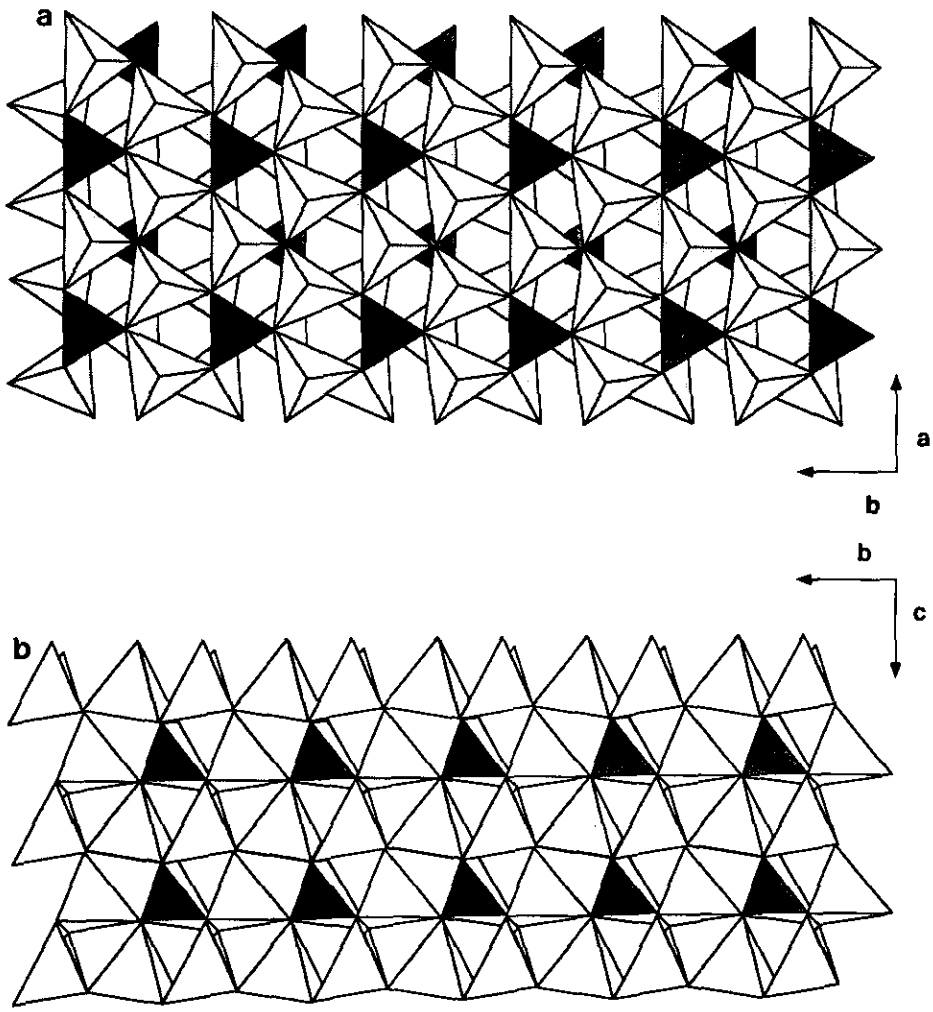

FIG. 3. Polyhedral crystal structure projections of (a) (001) and (b) (100) views of β-Li_3PO_4. The darker shaded tetrahedra are PO_4 and the lighter shaded tetrahedra are LiO_4.

occupied. The low occupation for the P site implies that a weaker scatterer is additionally present, such as Li and/or vacancies. Similarly for the Li-sites, the presence of some vacancies is suggested. Unfortunately, given the possibility of some Li ↔ P disorder combined with the presence of some vacancies on the tetrahedral sites, it is unlikely that a unique model can be determined on the basis of these refinements. Further models must be chemically reasonable and also be supported by the results of other physical measurements. Assume for the moment that some Li ↔ P disorder is present. To produce P—N=P linkages, as suggested by the HPLC results (see below), the Li ↔ P disorder must occur to avoid P—N=P linkages between tetrahedra sharing edges, e.g., Li(1) and Li(2) (Fig. 5a). This could be accomplished by the Li ↔ P disorder occurring among: (i) the Li(1) and P sites alone, (ii) the Li(2) and P sites alone, or (iii) all of the tetrahedral sites with correlated occupancies for neighboring Li(1) and Li(2) sites. Whichever pattern might be adopted, the overall framework nature of the tetrahedral linkage may produce some short length chains and rings of phosphate tetrahedra. Of the possible disorder schemes listed above, the occupations resulting from the Li(1) ↔ P are most consistent with the starting stoichiometry. This model yields a Li : P ratio of 2.88(4), 0.35 Li(2) vacancies per formula unit (pfu), 1.00(1) P pfu, 2.91(4) Li pfu, and 8% Li on the P site.

A summary of the refined structural parameters and agreement indices for the oxynitride (for the model with fully occupied tetrahedral sites, the other models used result in structural parameters that differ by no more than one esd) and γ-Li_3PO_4 samples are given in Table 1. The final positional parameters and isotropic displacement parameters are given in Table 2. Selected bond lengths and angles are given in Table 3. Included in the table for comparison are the corresponding values obtained from

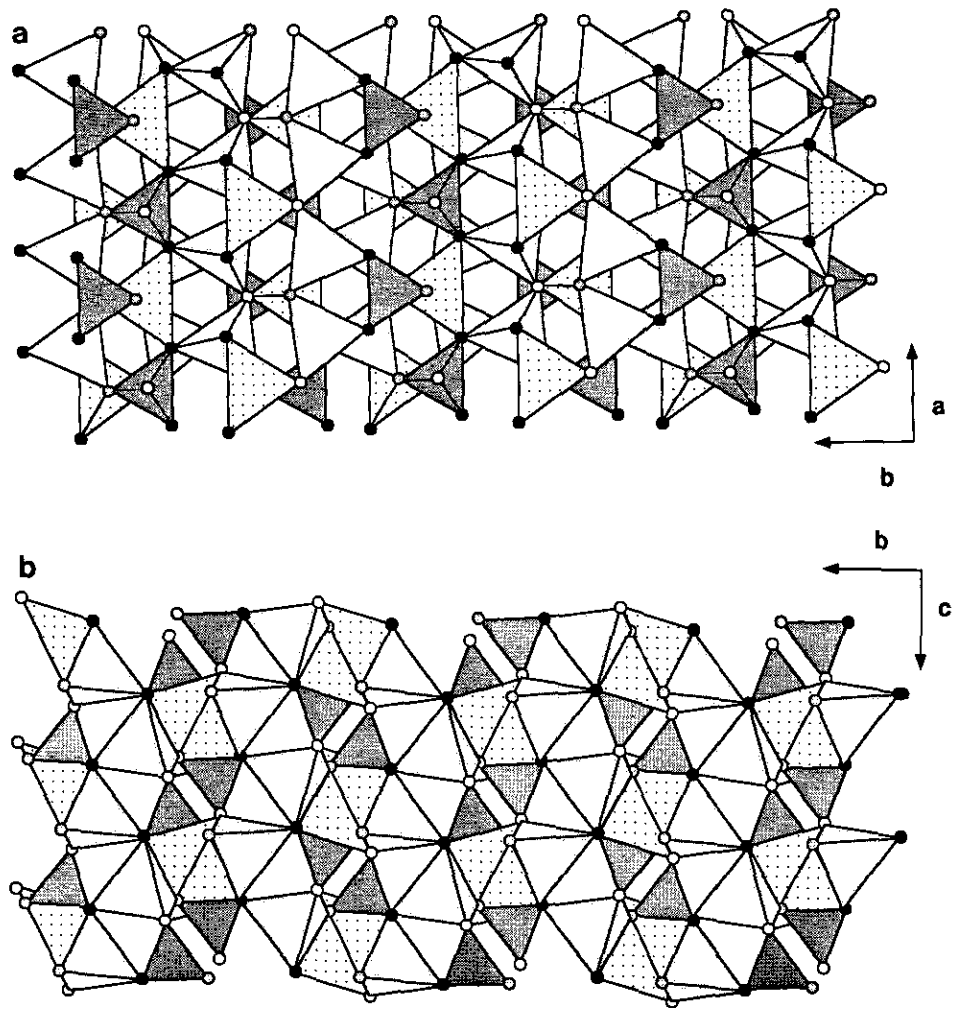

FIG. 4. Polyhedral crystal structure projections of (a) (001) and (b) (100) views of γ-Li_3PO_4 (subject of this study). The darkest shaded tetrahedra are PO_4 and the lighter shaded tetrahedra are LiO_4. The $Li(1)O_4$ and $Li(2)O_4$ tetrahedra are further distinguished by dark and light shading, respectively; and the three unique oxygens, O(1), O(2), and O(3) are identified by their black, gray, and white shading, respectively.

an X-ray single-crystal structure refinement for γ-Li_3PO_4 (11, 16). The observed, calculated, and difference neutron powder diffraction profiles are presented in Fig. 6. As judged by the peak widths, the crystallinity of $Li_{2.88}PO_{3.73}N_{0.14}$ is not as good as that of γ-Li_3PO_4.

Although the unit cell volume of $Li_{2.88}PO_{3.73}N_{0.14}$ is essentially identical to that of γ-Li_3PO_4, the cell dimensions exhibit small and anisotropic differences. The **a** and **b** cell dimensions both expand with $\Delta\mathbf{b} > \Delta\mathbf{a}$, while the **c** cell dimension contracts slightly. Substitution of nitrogen for oxygen should lengthen the Li–O and P–O bond distances due to the larger effective ionic radius of N^{3-} (1.32 Å, coordination number: IV) compared to that of O^{2-} (1.24 Å, coordination number: IV) (17). This is in fact the case, as shown in Table 3, except for the Li(1)–O(1), Li(1)–O(2), Li(2)–O(1), and P–O(2) bonds. Lengthening of the bonds is not consistent within a given tetrahedron because some of the bond distance changes are related to changes in the tetrahedral distortion. This distortion as measured by the deviation from the ideal tetrahedral bond angle increases in the series P < Li(1) ≪ Li(2) for γ-Li_3PO_4. With the introduction of nitrogen, both of the Li tetrahedra become less distorted while the P tetrahedra becomes more distorted in terms of the tetrahedral angle variances, yet the relative series remains the same. The bond valence sums ($V_i = \Sigma_j b_{ij}$; V_i, valence of atom i; b_{ij}, bond valence between atom i and neighboring atom j) to the oxygen sites in γ-Li_3PO_4 are all near the expected values, O(1) (1.97), O(2) (2.03), and O(3) (2.09), as computed using the bond valence parameters of Brown and Altermatt (18). Both O(1) and O(2) are involved in shared edges between LiO_4 tetrahedra, whereas O(3) is not (Fig. 5a). With the introduction of nitrogen, the bond valence sums change significantly: O(1) (1.93), O(2) (2.23), and

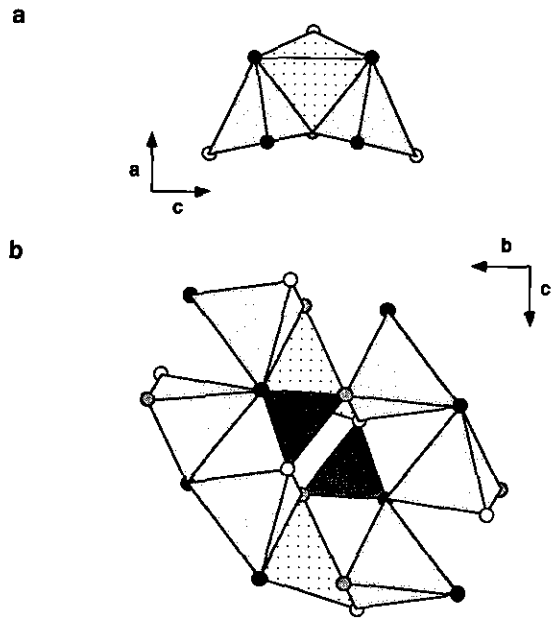

FIG. 5. The partial structure of γ-Li_3PO_4 showing: (a) edge sharing of two $Li(1)O_4$ with one $Li(2)O_4$ tetrahedra, (b) interconnection of PO_4 and LiO_4 tetrahedra. The shading of the tetrahedra is same as in Fig. 4.

O(3) (1.88). It is tempting to suggest that the underbonded O3 site might be due to oxygen vacancies and that the overbonded O2 site is enriched in nitrogen; however, no corroborating evidence such as consistent bond length changes can be offered.

Although the neutron diffraction data do not clearly indicate which of the oxygen sites are occupied by nitrogen, it is expected that one oxygen vacancy is created for every two nitrogen atoms incorporated into the structure in order to maintain charge balance. The formula $Li_{2.88}PO_{3.73}N_{0.14}$ implies that 3.25% of the anion sites are vacant: 1.75% are required to compensate for the 0.14 N per formula unit while the remainder are required to compensate for the 4.00% Li vacancies. The observed Li deficiency might be related to the N substitution assuming

TABLE 1
Crystal Data for Structural Refinements of $Li_{2.88}PO_{3.73}N_{0.14}$ and γ-Li_3PO_4

	$Li_{2.88}PO_{3.73}N_{0.14}$	γ-Li_3PO_4
R_{wp}	0.0531	0.0436
R_p	0.0453	0.0378
χ^2	1.789	1.232
a (Å)	6.1153(9)	6.1113(1)
b (Å)	10.469(1)	10.4612(2)
c (Å)	4.9195(8)	4.9208(1)
V (Å)	314.9(1)	314.60(2)

TABLE 2
Fractional Atomic Coordinates and Isotropic Displacement Parameters for $Li_{2.88}PO_{3.73}N_{0.14}$ and γ-Li_3PO_4

	x	y	z	U (Å^2)[a]
$Li_{2.88}PO_{3.73}N_{0.14}$				
Li(1)	0.496(1)	0.158(1)	0.313(1)	0.017(2)
Li(2)	0.75	0.421(1)	0.196(2)	0.017(3)
P	0.25	0.4147(6)	0.3060(1)	0.015(1)
O(1)	0.0401(6)	0.3429(3)	0.2167(8)	0.0133(9)
O(2)	0.25	0.0519(5)	0.2786(1)	0.008(1)
O(3)	0.75	0.0898(6)	0.1309(9)	0.016(1)
γ-Li_3PO_4				
Li(1)	0.5016(5)	0.1627(3)	0.3008(7)	0.0109(6)
Li(2)	0.75	0.4246(4)	0.2045(9)	0.0110(8)
P	0.25	0.4115(1)	0.3079(4)	0.0039(3)
O(1)	0.0441(1)	0.3418(1)	0.2054(2)	0.0060(3)
O(2)	0.25	0.0503(1)	0.2928(3)	0.0068(3)
O(3)	0.75	0.0896(1)	0.1223(2)	0.0056(3)

[a] The temperature factor in the expression for the structure factor is defined by $\exp[8\pi^2 U \sin\theta^2/\lambda^2]$.

that energetically favored defects involve the N atoms and exclude the full occupation of the Li sites.

The chromatogram of γ-Li_3PO_4 shown in Fig. 7a consists of a single orthophosphate anion peak (P_1) as expected for stoichiometric crystalline lithium orthophosphate. The chromatogram of $Li_{2.88}PO_{3.73}N_{0.14}$, however, shown in Fig. 7b contains additional features. The shoulder under the P_1 peak is probably due to nitrogen-substituted phosphate tetrahedra PO_3N. The other weak peaks are possibly due to phosphate anions linked together by —N= such as:

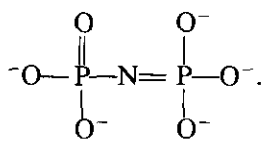

The much larger concentrations of PO_3N compared to other nitrogen-containing phosphate anions as judged from the HPLC data are consistent with the neutron structural refinement which suggests that nitrogen substitutes for oxygen in the tetrahedral anion sites similar to other nitride (AlN, (19)) and oxynitride compounds (Na_3WO_3N, (20)). Substitution of nitrogen at the oxygen sites is also indicated by the N_{1s} XPS spectrum shown in Fig. 8 if the major resolved component at 397.8 eV is attributed to nitrogen bonded to one phosphorus and three lithium atoms. This assignment is consistent with the XPS spectrum of wurtzite-type AlN (21) in which a single N_{1s} peak of nitrogen tetrahedrally bonded to four aluminum atoms appears at 396.4 (±0.1) eV. On the other hand, the component at 397.8 eV has been attributed to nitrogen bonded

TABLE 3
Selected Interatomic Distances (Å) and Angles (°) for $Li_{2.88}PO_{3.73}N_{0.14}$ and γ-Li_3PO_4

	$Li_{2.88}PO_{3.73}N_{0.14}$[a]	γ-Li_3PO_4[a]	γ-Li_3PO_4[b]
PO_4 tetrahedron			
P–O(1)	1.538(5)	1.539(1)	1.553(7)
P–O(1)	1.538(5)	1.539(1)	1.553(7)
P–O(2)	1.497(8)	1.533(2)	1.552(7)
P–O(3)	1.583(7)	1.547(2)	1.543(8)
Mean	1.539	1.540	1.550
O(1)–P–O(1)	111.4(4)	109.6(1)	110.0
O(1)–P–O(2)	112.5(2)	110.0(8)	109.8
O(1)–P–O(3)	106.2(2)	108.8(8)	108.7
O(1)–P–O(2)	111.4(4)	110.0(8)	109.8
O(1)–P–O(3)	112.5(2)	108.8(8)	108.7
O(2)–P–O(3)	107.5(4)	109.3(1)	109.5
Mean	110.3	109.4	109.4
P–O(1)–Li(1)	119.4(4)	119.5(1)	119.5
P–O(1)–Li(1)	114.2(4)	116.2(1)	115.3
P–O(1)–Li(2)	123.5(5)	122.1(1)	122.6
P–O(2)–Li(1)	126.8(4)	125.5(1)	124.9
P–O(2)–Li(1)	126.8(4)	125.5(1)	124.9
P–O(2)–Li(2)	113.4(5)	116.2(1)	116.4
P–O(3)–Li(1)	118.4(3)	117.5(1)	117.9
P–O(3)–Li(1)	118.4(3)	117.5(1)	117.9
P–O(3)–Li(2)	114.1(5)	115.7(1)	115.6
$Li(1)O_4$ tetrahedron			
Li(1)–O(1)	2.001(1)	1.951(3)	1.95(1)
Li(1)–O(1)	1.999(9)	2.008(3)	2.00(2)
Li(1)–O(2)	1.886(1)	1.936(3)	1.94(2)
Li(1)–O(3)	1.936(1)	1.913(3)	1.89(4)
Mean	1.956	1.952	1.94
O(1)–Li(1)–O(1)	105.1(5)	106.2(1)	106.2
O(1)–Li(1)–O(2)	117.4(6)	117.6(1)	116.8
O(1)–Li(1)–O(3)	109.6(5)	112.7(1)	112.9
O(1)–Li(1)–O(2)	117.4(6)	96.2(1)	95.3
O(1)–Li(1)–O(3)	109.6(5)	110.0(1)	111.2
O(2)–Li(1)–O(3)	112.1(6)	112.2(1)	112.5
Mean	111.9	109.2	109.1
$Li(2)O_4$ tetrahedron			
Li(2)–O(1)	1.974(7)	1.995(2)	1.97(1)
Li(2)–O(1)	1.974(7)	1.995(2)	1.97(1)
Li(2)–O(2)	2.106(1)	2.043(5)	2.02(3)
Li(2)–O(3)	1.944(1)	1.926(4)	1.95(2)
Mean	2.000	1.990	1.97
O(1)–Li(2)–O(1)	129.6(8)	128.5(2)	128.9
O(1)–Li(2)–O(2)	95.0(5)	93.3(1)	93.7
O(1)–Li(2)–O(3)	111.7(4)	112.8(1)	112.4
O(1)–Li(2)–O(2)	95.0(5)	93.3(1)	93.7
O(2)–Li(2)–O(3)	108.0(7)	108.8(2)	108.7
Mean	108.5	108.3	108.3
Li(1)–O(1)–Li(1)	102.3(3)	101.3(1)	101.4
Li(1)–O(1)–Li(2)	108.1(5)	106.7(1)	106.4
Li(1)–O(1)–Li(1)	81.0(5)	83.7(1)	84.2
Li(1)–O(2)–Li(1)	105.8(7)	105.1(2)	106.4
Li(1)–O(2)–Li(2)	80.3(4)	84.3(1)	84.4
Li(1)–O(2)–Li(2)	80.3(4)	84.3(1)	84.4
Li(1)–O(3)–Li(1)	106.7(6)	105.0(2)	104.2
Li(1)–O(3)–Li(2)	97.5(4)	98.9(1)	98.9
Li(1)–O(3)–Li(2)	97.5(4)	98.9(1)	98.9

[a] Present work.
[b] Generated using the atomic coordinates and cell parameters given in Ref. (16).

to two phosphorus atoms, P—N=P, in many studies of oxynitride glasses (22, 23) based on the proposed assignment of the N_{1s} spectrum of $P_3N_5H_x$ by Veprek *et al.* (24). The formation of a small concentration of P—N=P linkages is apparently due to some Li ↔ P disorder in the structure, but it is unreasonable to assign the major N_{1s} component to this type of nitrogen given the more reasonable alternative described above. Moreover, to be consistent with the assignment by Veprek *et al.* (24) and with all of the other studies of phosphorus nitride glasses in which this assignment of the N_{1s} spectrum was used, the resolved N_{1s} component at 399.7 eV shown in Fig. 8 should be attributed to nitrogen bonded to three P atoms,

$$\text{P—N} < \begin{matrix} \text{P} \\ \text{P} \end{matrix}.$$

This type of N bonding is consistent with the average crystal structure if some Li ↔ P disorder is present.

Marchand *et al.* (25) report a similar asymmetric N_{1s} peak in the X-ray photoelectron spectrum of polycrystalline PON. This material has the cristobalite structure, and only one type of nitrogen with the doubly coordinated structure P—N=P is expected. Marchand *et al.* (25) attribute the 399.7 eV component to the presence of an amorphous PON phase in their sample; judging from the relative intensities of the two components, the sample must have contained about 30% of the amorphous phase. In the case of $Li_{2.88}PO_{3.73}N_{0.14}$, the 399.7 eV component also contributes about 30% to the total intensity of the N_{1s} spectrum, but to assign this peak to a second phase present at the 30% level is unreasonable because no evidence for a second phase was detected in the X-ray or neutron diffraction measurements. Results for Li_3N dis-

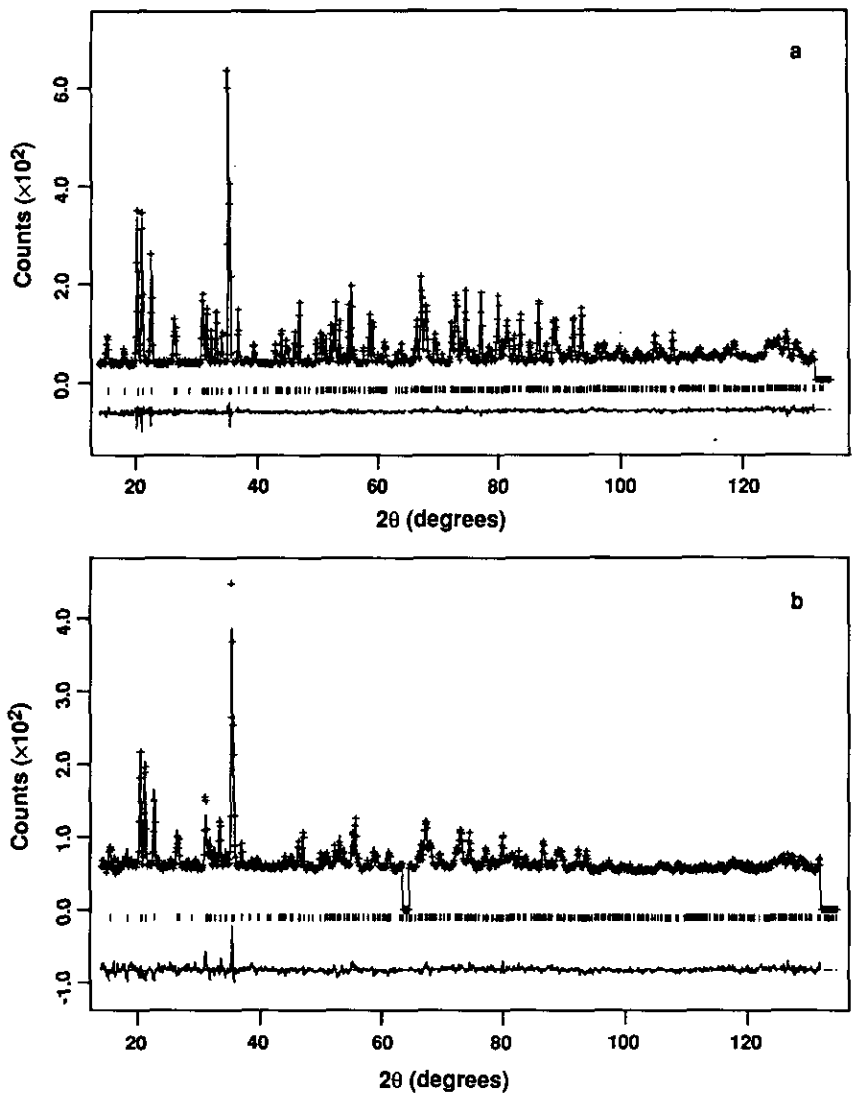

FIG. 6. Observed, calculated, and the difference neutron diffraction profiles for (a) γ-Li_3PO_4 and (b) $Li_{2.88}PO_{3.73}N_{0.14}$ (λ = 1.416 Å). The observed data are indicated by (+), and the calculated profile is the continuous solid line in the same field. The short vertical lines below the profiles mark the positions of all possible Bragg reflections, and the bottom curve is the difference between the observed and calculated intensity (plotted using the same vertical scale as the observed and calculated profiles).

cussed below suggest that the 399.7 eV component might be due to a nitrogen-containing species formed by surface reaction.

As shown in Fig. 8, there are two additional weak features in the N_{1s} region at 404.2 and about 395.4 eV. The former is observed in photoelectron spectra of lithium phosphorus oxynitride thin films (1, 2). The origin of these two weak peaks is not known, but they are believed to be due to the 1*s* state of nitrogen in different chemical environments. The N_{1s} spectrum of polycrystalline Li_3N shown in Fig. 9 was resolved to four peaks located at 405.4, 399.2, 397.6, and 395.2 eV, respectively. There is only one type of nitrogen in the Li_3N structure, and the main feature at 397.6 eV is probably due to this nitrogen which is bonded to eight lithium atoms (26) because the relative intensity of this peak decreases with decreasing electron escape angle, although the relative intensity of other minor two peaks at 405.4 and 395.2 also decreases with decreasing electron escape angle. The increase in peak intensity with decreasing electron escape angle at 399.2 eV suggests that this peak might be due to the 1*s* states of nitrogen due to surface contamination of the highly reactive Li_3N.

Examples of the impedance spectra of γ-Li_3PO_4 and $Li_{2.88}PO_{3.73}N_{0.14}$ are shown in Fig. 10. These spectra are characteristic of a single-phase ionic conductor sandwiched between blocking metal contacts (1). The sample resistance R can be accurately determined from the mea-

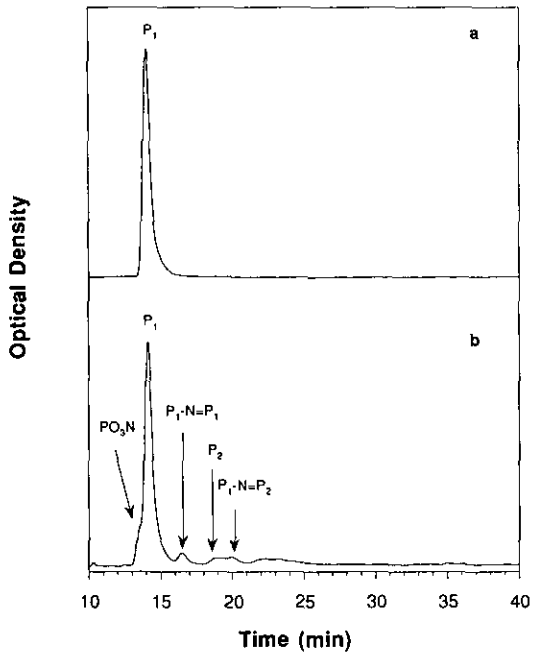

FIG. 7. Chromatograms of γ-Li_3PO_4 (a) and $Li_{2.88}PO_{3.73}N_{0.14}$ (b).

sured impedance by selecting the value of Re(Z) at the frequency at which $-$Im(Z) goes through a local minimum. The ionic conductivity is then calculated from $\sigma = d/(A \cdot R)$ where d is the sample thickness and A is the area of the Pt contact. Graphs of σT vs $1/T$ for $Li_{2.88}PO_{3.73}N_{0.14}$ and γ-Li_3PO_4 are displayed in Fig. 10. Because of the high resistivity of the γ-Li_3PO_4 sample at low temperatures, reliable data could not be obtained below about 250°C. Extrapolation of the high temperature data to lower

TABLE 4

Comparison of Conductivity at 25°C and Activation Energy for Polycrystalline and Thin Film Lithium Phosphorus Oxynitride Materials

Sample	$\sigma_{25°C}$ (S · cm^{-1})	E_a (eV)	σ_0 (S · cm^{-1} · K)
Polycrystalline			
γ-Li_3PO_4	4.2×10^{-18}[a]	1.24	1.0×10^6
$Li_{2.88}PO_{3.73}N_{0.14}$	1.4×10^{-13}[a]	0.97	9.6×10^5
Thin film[b]			
$Li_{2.7}PO_{3.9}$	6.6×10^{-8}	0.68	6.0×10^6
$Li_{3.3}PO_{3.9}N_{0.17}$	2.4×10^{-6}	0.56	1.5×10^6

[a] Extroplated data.
[b] Ref. (1).

temperatures, however, is in good agreement with previously reported results (27–30). The calculated activation energies E_a and the preexponential factor σ_0 in the Arrhenius equation $\sigma T = \sigma_0 \exp(-E_a/RT)$ and the conductivities for $Li_{2.88}PO_{3.73}N_{0.14}$ and γ-Li_3PO_4 at 25°C are listed in Table 4. The results from our previous studies of amorphous lithium phosphorus oxynitride thin films with similar compositions are included for comparison.

The data in Table 4 and Fig. 11 show that the introduction of a small concentration of nitrogen into the structure of γ-Li_3PO_4 increases the conductivity by several orders of magnitude. A comparison of the values of E_a and σ_0 suggests that the higher conductivity of $Li_{2.88}PO_{3.73}N_{0.14}$ is due to a lower activation energy, i.e., to an increase in the Li^+ mobility. In the γ-Li_3PO_4 structure, the Li^+ ions occupy tetrahedral sites in a framework structure formed by the P and O (11, 16, 31), and all of the Li sites

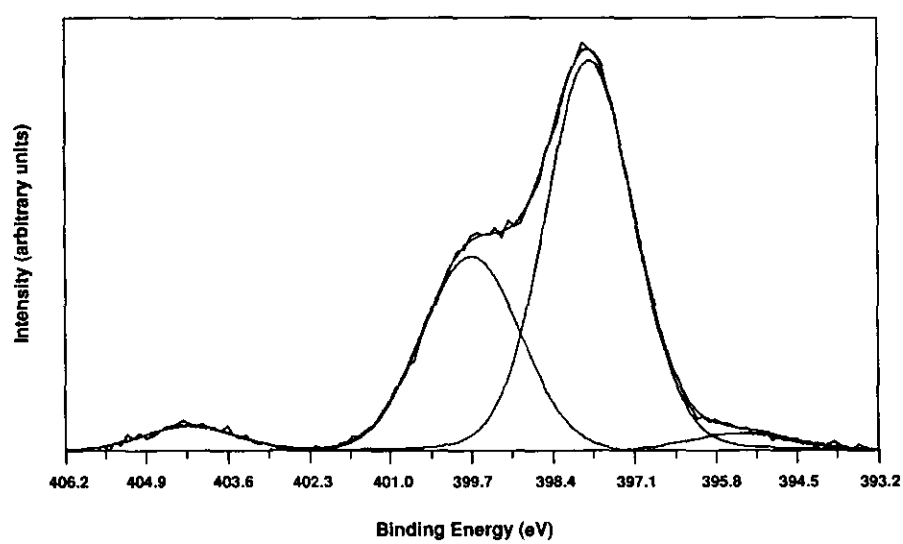

FIG. 8. X-ray photoelectron spectrum of $Li_{2.88}PO_{3.73}N_{0.14}$ in the N_{1s} region. The jagaged line is the original spectrum, and the smoothed lines are the fitted curves representing different environments of nitrogen.

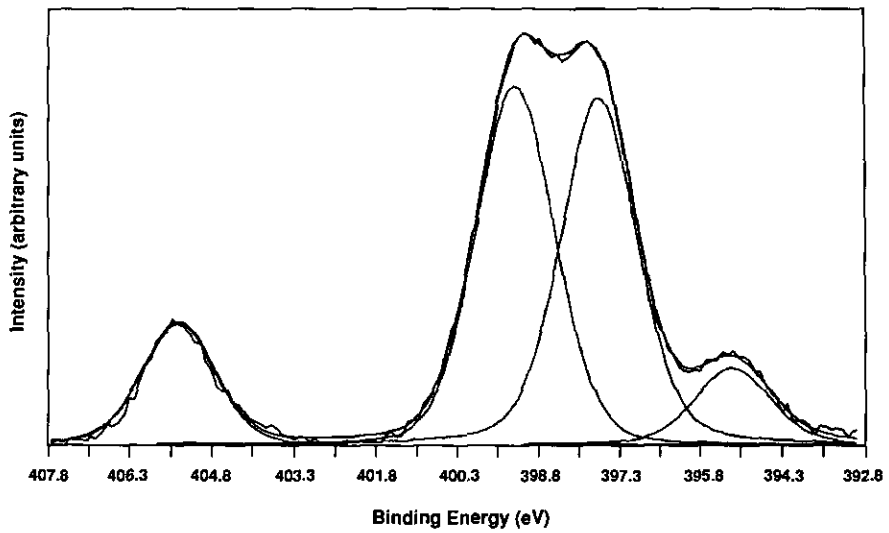

FIG. 9. X-ray photoelectron spectrum of Li_3N in the N_{1s} region. The jagged line is the original spectrum, and the smoothed lines are the fitted curves representing different environments of nitrogen.

are fully occupied. On the other hand, in $Li_{2.88}PO_{3.73}N_{0.14}$, a large concentration of vacancies at the Li-sites (4.00%) and the anion sites (3.25%) were created as the result of the substitution of nitrogen for oxygen. These defects likely result in a decrease in the activation energy for lithium ion conduction. The orders-of-magnitude increase in the ionic conductivity of solid solutions of Li_3PO_4 and Li_4SiO_4 compared to either end member was also attributed to a high lithium vacancy concentration (27–30). In addition, the replacement of smaller O^{2-} ions with larger N^{3-} ions increases the size of the small bottleneck through which the lithium ions must pass in γ-Li_3PO_4

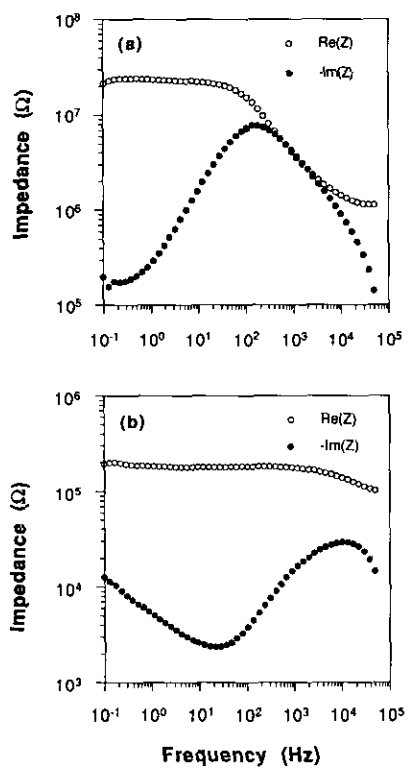

FIG. 10. Impedance spectra of (a) γ-Li_3PO_4 and (b) $Li_{2.88}PO_{3.73}N_{0.14}$ measured at 270°C.

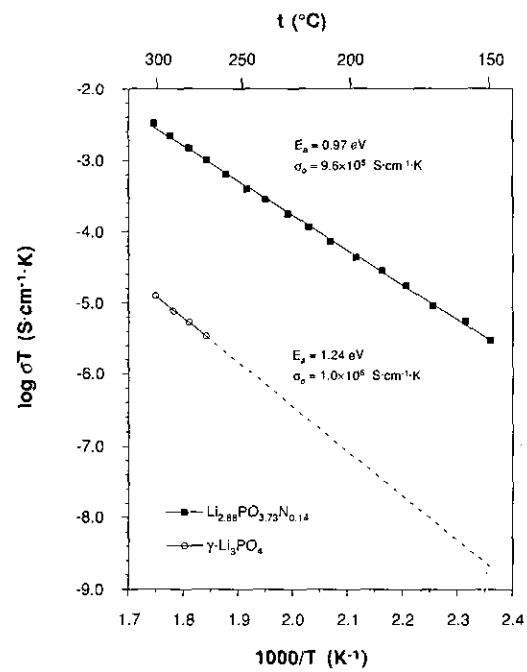

FIG. 11. Arrhenius plots of the ionic conductivity of γ-Li_3PO_4 and $Li_{2.88}PO_{3.73}N_{0.14}$. The solid lines are graphs of $\sigma T = \sigma_0 \exp(-E_a/RT)$. The activation energies E_a and the preexponential factor σ_0 were fit by least-squares to the data.

(32) as evidenced by the increase of **a** and **b** unit-cell parameters (Table 1). This also lowers the activation energy. As shown in Table 4, the formation of an amorphous phase of lithium orthophosphate and lithium phosphorus oxynitride achieved in film deposition at ambient temperatures results in a significant increase in lithium ion mobility.

CONCLUSIONS

Polycrystalline lithium phosphorus oxynitride $Li_{2.88}PO_{3.73}N_{0.14}$ can be prepared by the solid state reaction between Li_3N and $LiPO_3$. The structure of this material is similar to that of γ-Li_3PO_4 with a slightly larger unit cell. The ionic conductivity of $Li_{2.88}PO_{3.73}N_{0.14}$ is several orders of magnitude higher than that of γ-Li_3PO_4 due to its relatively lower activation energy which is attributed to the Li site and anion site vacancies and the expanded **a** and **b** cell dimensions.

ACKNOWLEDGMENTS

The authors thank Dr. N. J. Dudney for her critical reading of the manuscript and helpful suggestions. This research was sponsored by the Division of Materials Sciences, U. S. Department of Energy under Contract DE-AC05-84OR21400 with Martin Marietta Energy Systems, Inc. B. W. and B. S. K. were supported by an appointment to the Oak Ridge National Laboratory Postdoctoral Research Program administered by the Oak Ridge Institute for Science and Education. We also thank Dr. D. P. Hoffmann and Mr. J. Harrison for making XPS available and for their generous assistance.

REFERENCES

1. J. B. Bates, N. J. Dudney, G. R. Gruzalski, R. A. Zuhr, A. Choudhury, C. F. Luck, and J. D. Robertson, *Solid State Ionics* **53–56,** 647 (1992).
2. J. B. Bates, G. R. Gruzalski, N. J. Dudney, and C. F. Luck, *in* "Proceedings, 35th Power Sources Symp," p. 337. 1992
3. J. B. Bates, N. J. Dudney, G. R. Gruzalski, C. F. Luck, X-H. Yu, and S. D. Jones, *Solid State Technol.* **July,** 59 (1993).
4. K. Juszczyk and S. Podsialdo, *Pr. Nauk. Akad. Ekon. im Oskara Langego Warclawiu* **526,** 231 (1990).
5. H. E. Swanson, M. C. Morris, E. H. Evans, and L. Ulmer, *Natl. Bur. Stand. Monogr. U. S.* **25,** 39 (1964).
6. B. C. Chakoumakos, J. A. Fernandez-Baca, and L. A. Boatner, *J. Solid State Chem.* **103,** 105 (1993).
7. A. C. Larson and R. B. Von Dreele, "GSAS—General Structure Analysis System," Rept. LA-UR-86-748, Los Alamos National Laboratory, Los Alamos, New Mexico, 1990.
8. H. M. Rietveld, *J. Appl. Crystallogr.* **2,** 65 (1969).
9. P. Thompson, D. E. Cox, and J. B. Hastings, *J. Appl. Crystallogr.* **20,** 79 (1987).
10. V. F. Sears, "Methods of Experimental Physics, Vol 23, Part A" (K. Skold and D. L. Price, Ed.), p. 521. Academic Press, Orlando, 1986.
11. C. Keffer, A. Mighell, F. Mauer, H. Swanson, and S. Block, *Inorg. Chem.* **6,** 119 (1969).
12. B. C. Sales, R. S. Ramsey, J. B. Bates, and L. A. Boatner, *J. Non-Cryst. Solids* **87,** 137 (1986).
13. B. Wang, B. S. Kwak, B. C. Sales, and J. B. Bates, in preparation.
14. L. Boukbir and R. Marchand, *Rev. Chim. Min.* **23,** 343 (1986).
15. E. Reculeau, A. Elfakir, and M. Quarton, *J. Solid State Chem.***79,** 205 (1989).
16. W. H. Baur, *Inorg. Nucl. Chem. Lett.* **16,** 525 (1980).
17. R. D. Shannon, *Acta Crystallogr. Sect. A* **32,** 751 (1976).
18. I. D. Brown and D. Altermatt, *Acta Crystallogr. Sect. B* **24,** 244 (1985).
19. W. G. Wyckoff, *Cryst. Struct.* **1,** 112 (1963).
20. S. H. Elder, F. J. DiSalvo, J. B. Parise, J. A. Hriljac, and J. W. Richardson, Jr., *J. Solid State Chem.* **108,** 73 (1994).
21. H. M. Liao, R. N. S. Sodhi, and T. W. Coyle, *J. Vac. Sci. Technol. A* **11,** 2681 (1993).
22. R. Marchand, D. Agliz, L. Boukbir, and A. Quemerais, *J. Non-Cryst. Solids* **103,** 35 (1988).
23. R. K. Brow, M. R. Reidmeyer, and D. E. Day, *J. Non-Cryst. Solids* **99,** 178 (1988).
24. S. Veprek, S. Iqbal, J. Brunner, and M. Scharli, *Philos. Mag.* **43,** 527 (1981).
25. R. Marchand, Y. Lauqent, and A. Quemerais, *Riv. Stn. Sper. Vetro Murano, Italy* **5,** 101 (1990).
26. A. Rabenau and H. Schulz, *J. Less-Common Met.* **50,** 155 (1976).
27. Y-W. Hu, I. D. Raistrick, and R. A. Huggins, *J. Electrochem. Soc.* **124,** 1240 (1977).
28. R. A. Huggins, *Electrochim. Acta.* **22,** 773 (1977).
29. R. D. Shannon, B. E. Taylor, A. D. English, and T. Berzins, *Electrochim. Acta.* **22,** 783 (1977).
30. B. Zhu, B-E. Mellander, and J. Chen, *Mater. Res. Bull.* **28,** 321 (1993).
31. J. Zemann, *Acta Crystallogr.* **13,** 863 (1960).
32. H. Y-P. Hong, *Mater. Res. Bull.* **13,** 117 (1978).